Modeling of Fluidized Bed Reactors With Two Reaction Zones

Jorge Gascón, Carlos Téllez, and Javier Herguido,
Dept. of Chemical and Environmental Engineering, Univ. of Zaragoza, 50009 Zaragoza, Spain

Hugo A. Jakobsen
Dept. of Chemical Engineering, Norwegian Univ. of Science and Technology, N-7491 Trondheim, Norway

Miguel Menéndez
Dept. of Chemical and Environmental Engineering, Univ. of Zaragoza, 50009 Zaragoza, Spain

In the present work, a mathematical model is presented for simulating fluidized bed reactors with two zones. Two reactions have been chosen as being representative of the two main uses of this kind of catalytic reactors: propane dehydrogenation and n-butane partial oxidation. The experimental data obtained in a bench scale plant have been simulated using the same fluid-dynamic model for both reactions, based generally on the description of the three-phase model and kinetic models previously developed. By applying those models, most of the trends experimentally checked can be well forecast, gaining a better understanding of the behavior of reactors and reactions. On the other hand, some parameters that could not be determined experimentally, such as the velocity of solid circulation or the oxidation state of the VPO catalyst, turned out to be among the most important reactor-related variables. © 2006 American Institute of Chemical Engineers *AIChE J,* 52: 3911–3923, 2006
Keywords: propane, propene, n-butane, maleic anhydride, dehydrogenation, partial oxidation, TZFBR, ICFBR

Introduction

Some features of fluidized bed reactors, such as the temperature uniformity along the bed, can be positively exploited in chemical reaction processes. Catalyst circulation through the bed allows the separation of the bed into two different reaction zones (that is, two different atmospheres) in the same reactor vessel by feeding the reactants separately at different bed points, while at the same time the catalyst will continuously move between both zones.[1,2] This provides an opportunity to upgrade some catalytic processes where the catalyst properties

allow the use of semi-continuous reaction systems, where catalyst oxidation and reduction may be carried out sequentially, or the use of complex reaction set-ups, where two reactors are used and the solid catalyst is continuously transferred between them. Two classes of such processes are non oxidative dehydrogenations and selective oxidations.

Catalyst deactivation by coking is the most common problem of non-oxidative dehydrogenation processes. To remove the coke deposits from the catalyst surface, combustion with oxygen-diluent mixtures is often carried out off-line, either in the same or separate reactors, after purging the flammable hydrocarbon gases. In any case, the downtime for regeneration represents a significant economic penalty. Various processes have been proposed for continuously regenerating the catalyst, such as the Snamprogetty Propane fluidized bed dehydrogena-

Correspondence concerning this article should be addressed to M. Menéndez at qtmiguel@unizar.es.
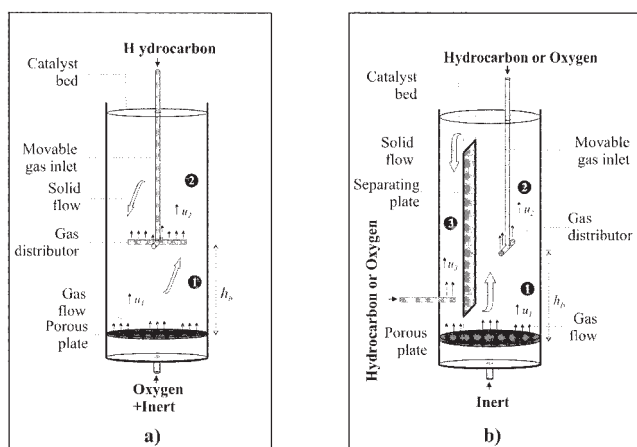
Figure 1. Reactor configurations used in this work.

(a) TZFBR; (b) ICFBR. u_1, u_2, and u_3 denote the different gas velocities in different parts of the bed.

tion (FBD-3),[3,4] where two connected fluidized bed reactors are used. Another problem associated with industrial dehydrogenation reactors is how to supply the huge quantity of heat needed by the reaction while maintaining a careful control of the temperature in order to minimize the formation of other products (cracking) and maximize the yield to the desired product. In some processes, this heat is supplied by the sensible heat stored in the catalyst bed during the regeneration step, while in other cases additional heat is provided by direct fuel combustion.

Usually, gas phase catalytic oxidations involve feeding a reactant with an oxygen-diluent mixture to a fixed or fluidized bed catalytic reactor. Some drawbacks are associated with the use of single fixed or fluidized beds; the most important is the low hydrocarbon concentration that must be fed in order to avoid flammability limits (maximum concentration of butane in air around 1-2%). Fluidized beds are the preferred reactors for large scale plants[5-7] because they allow a more efficient heat removal and a better temperature control, and because higher feed concentrations are possible, up to 4% butane in air, since the fluidized catalyst acts as a flame arrester, quenching the free radicals.[8] Another drawback is that it is not possible to control the oxidation state of the catalyst in order to obtain the most suitable product distribution. The fact that the lattice of a catalytic oxide can act as an oxygen stock and transfer this oxygen in oxidation reactions under suitable conditions allows the development of new processes where the oxygen required for the oxidation is provided by the catalyst itself, which is reoxidized in a separate step. The best known example is the Circulating Fluid Bed Reactor (CFBR), consisting of a riser-regenerator system, developed by Dupont.[7,9]

During the last decade, our group has been researching alternative processes to both the CFBR and unsteady state operations in one single vessel. The main target has been to take advantage of the simplicity of using one single vessel and that of the continuous operation of circulating systems. To this end, we have developed two kinds of fluidized bed reactors that use separated oxygen and hydrocarbon feeds. The first, the two zone fluidized bed reactor (TZFBR, Figure 1a) consists of a fluidized bed where the oxidizing mixture is fed to the lower

part of the reactor, while the hydrocarbon is fed in an intermediate part of the bed. In the second, the internal circulating fluidized bed reactor (ICFBR, Figure 1b), the solid flow is governed by a mechanism similar to that existing in the well-known airlift reactor employed in microbial fermentations. The reactor is divided into two zones by a vertical wall that allows transfer of solids between both zones through connections in the lower and the upper parts of the bed. Because of the different gas velocity in each zone, a pressure gradient appears, causing solid flow between both parts of the bed.

These new reactors have been satisfactorily tested for the oxidative coupling of methane,[10] the oxidative dehydrogenation of n-butane,[11,12] the catalytic dehydrogenation of n-butane[13] and propane,[1] and the n-butane partial oxidation to maleic anhydride.[2] A detailed review of the use of the TZFBR and the ICFBR has been recently published.[14]

The main objective of the present work is the improvement and further development of a mathematical model previously proposed[12,15] for simulating the behavior of the fluidized bed reactors described above, with the aim of understanding the system as well as predicting the effect of the main related variables. Two reactions not considered in the previous simulation studies have been chosen, propane dehydrogenation as representative of a catalytic dehydrogenation and n-butane oxidation to maleic anhydride as representative of a partial oxidation, in order to generalize the behavior of the reactors independent of the reaction carried out inside them. Using for both cases the same fluid-dynamic model and kinetic models previously developed by our group for each reaction,[16,17] the experimental data obtained in our bench scale plant for the catalytic dehydrogenation of propane over a Cr_2O_3/Al_2O_3 catalyst[1] and the n-butane partial oxidation over a commercial VPO catalyst[2] have been simulated.

Mathematical Reactor Model

The development of a mathematical model is necessary in order to gain a better understanding of the behavior of the reactor and also for further optimization and scale up. This model is based on that previously developed[15] for a TZFBR, to which several improvements were added in the model presented later[12] for the simulation of an ICFBR. The main difference between the reactors is that in the TZFBR the flow of solid between both reaction zones (the solid interchange between zones) is produced only by the transport in the wake of the bubbles and the subsequent drop of solid in the emulsion phase. In the ICFBR, the main flow of solid is that appearing between the two interconnected beds due to a difference in the pressure drop of the gas when passing through each bed. The solid transport between beds is modeled according to the results from a previous fluid dynamic study using a cold model.[12]

The fluid dynamic model considered includes the existence of three different zones: bubble, wake, and emulsion.[18] The solid in the wake is raised with the bubble. When the bubble reaches the bed surface, the solid in the wake is incorporated into the emulsion. Bubbles are, therefore, responsible for the solid mixing in the fluidized bed.

The solid exchange between wake and emulsion was also considered. The same concentration of each gaseous compound was assumed in the bubbles and in the wake (the gas in both being well mixed). It will also be assumed that the gas con-

centration in the cloud surrounding the bubble is the same as that in the emulsion. The gas exchange between bubbles and emulsion will be considered, as well as the solid exchange. The following additional simplifications have been considered in the gas flow model:

(a) Isothermal bed. This is a common assumption due to the high degree of solid mixing. This has been experimentally checked.[1,2]

(b) The gas velocity and the porosity in the emulsion phase are those measured experimentally in minimum fluidization conditions.

(c) The hydrocarbon is mixed instantaneously at the feeding point with the inert and oxygen streams. The hydrocarbon is thus distributed proportionally between the bubble and the emulsion phases (this assumption provided a better fit to the experimental results than assuming that the hydrocarbon forms only new bubbles). This was also assumed in the model previously developed by our group[12] and is a suitable assumption when the reaction is not very fast.[19]

Therefore, in order to describe both models, their various parts (gas and solid flow) will be discussed in some detail, and the resulting equations shown later. Two reactions have been simulated for both reactors (TZFBR and ICFBR): propane dehydrogenation and oxidation of n-butane to maleic anhydride. As has been explained above, the main difference between the reactors lies in the solid flow along the bed; therefore, a common explanation is given for the fluid dynamic model, with special attention being drawn to the differences between the reactors.

Fluid-dynamic model

The model for the gas flow follows mainly the description of the three-phase model.[18] We have considered that the gas rises in the emulsion at a relative velocity equal to the minimum fluidization velocity, and that the remaining gas rises in the bubbles. The gas in the bubbles, according to the Davidson[20] bubble model, is continuously being recirculated to the bubble (and, thus, the gas inside the bubble is well mixed), penetrating the emulsion only slightly. The bubble carries with its rising movement a certain amount of solid, called the wake.[21] The equations employed to estimate the bubble size, bubble rising velocity, gas exchange coefficient between bubble and emulsion, the solid exchange coefficient between wake and emulsion, and other parameters that appear in the fluid dynamic model are given in Table 1.

A value of 0.15 has been considered for f_w (volumetric fraction of wake in bubbles), roughly what may be expected for the bubble diameter (d_b) calculated. Although some attempts to correlate f_w with d_b have been published,[22,23] the large dispersion in the experimental values makes it difficult to predict this parameter with precision. However, a previous parametric study[24] showed that the variation of f_w between 0.05 and 0.15 only results in small changes (less than one percentage point) in the conversion or selectivity values predicted by the model.

The correlation of Darton et al.[25] has been used to calculate the bubble diameter in many previous studies,[12] for relatively coarse particles, such as Geldart's Group B or D powders. For group A particles, where both bubble coalescence and splitting are important, Horio and Nonaka's correlation[26] is more ap-

Table 1. Equations Employed in the Fluid Dynamic Model

Bubble diameter[26]

$$\left(\frac{\sqrt{d_B} - \sqrt{d_{Be}}}{\sqrt{d_{B0}} - \sqrt{d_{Be}}}\right)^{1-\gamma_M/\eta} \left(\frac{\sqrt{d_B} - \sqrt{\delta}}{\sqrt{d_{B0}} - \sqrt{\delta}}\right)^{1-\gamma_M/\eta} = \exp\left(-0.3\frac{z-z_0}{D_t}\right)$$

$$d_{B0} = \frac{3.77(u - u_{mf})^2}{g} \text{ for porous plates}$$

$$d_{Bm} = 1.49 \, g^{-0.2}[(u - u_{mf})\pi D_t^2]^{0.4}$$

$$\delta/D_t = \frac{(\gamma_m + \eta)^2}{4}$$

$$\eta = (\gamma_m^2 + 4d_{Bm}/D_t)^{0.5}$$

$$d_{Be}/D_t = [-\gamma_m + (\gamma_m^2 + 4d_{Bm}/D_t)^{0.5}]^2/4$$

$$\gamma_m = 7.22 \cdot 10^{-3} \, (D_t/g)^{0.5}/u_{mf}^{1.2}$$

Bubble rising velocity[27,28]

$$u_B = f \cdot \alpha \cdot u_B + K_B \cdot \sqrt{g \cdot d_B}$$

$$f = \frac{1 - \exp(-2 \cdot (u_0/u_{mf} - 1))}{1 - \exp(-9 \cdot \alpha \cdot u_B)}$$

Gas exchange between bubble and emulsion[18]

$$K_{bc} = 4.5 \cdot \left(\frac{u_{mf}}{d_B}\right) + 5.85 \cdot \left(\frac{D^{0.5} \cdot g^{0.25}}{d_B^{5/4}}\right)$$

$$K_{ce} = 6.78 \cdot \left(\frac{\varepsilon_{mf} \cdot D \cdot u_B}{d_B^3}\right)^{1/2}$$

Diffusion coefficient: D[29]

Chapman-Enskog equation

Solid exchange between wake and emulsion[30]

$$K_w = \begin{cases} \dfrac{0.075 \cdot (u_0 - u_{mf})}{u_{mf} \cdot d_B} & \text{if } u_0/u_{mf} \leq 3 \\[2ex] \dfrac{0.15}{d_B} & \text{if } u_0/u_{mf} > 3 \end{cases}$$

Volumetric fraction of bubbles in the bed[18]

$$\alpha = \frac{u_0 - (1 - \alpha - \alpha \cdot f_w) \cdot u_{mf}}{u_B} \approx \frac{u_0 - u_{mf}}{u_B}$$
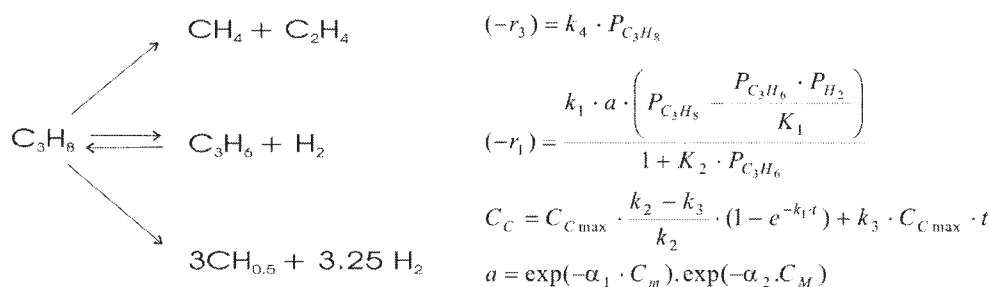
propriate and is thus chosen in the present work for the estimation of bubble size.

A parametric study of the initial bubble size has been performed with the aim of estimating the optimum value of this parameter. According to Horio and Nonaka,[26] the initial bubble diameter for a porous plate must be calculated by using the equation given in Table 1, but results obtained by this equation for the experimental conditions used in this work forecast an initial bubble diameter that is too small (<0.05 mm). Since the initial bubble diameter must be at least as large as the particle diameter (0.2 mm), the initial bubble diameter was varied between 0.2 and 2 mm, the best results being obtained for a value of 0.5 mm.

Kinetic models

Propane Dehydrogenation.   The proposed kinetic model for propane dehydrogenation over a Cr_2O_3/Al_2O_3 catalyst has been previously published.[16] As is shown in Figure 2a, a Langmuir–Hinshelwood mechanism is proposed for the main reaction, while a potential kinetic equation is used for the formation of light hydrocarbons (mainly methane and ethyl-

Catalytic propane dehydrogenation

$$CH_4 + C_2H_4$$

$$(-r_3) = k_4 \cdot P_{C_3H_8}$$

$$C_3H_8 \rightleftharpoons C_3H_6 + H_2$$

$$(-r_1) = \frac{k_1 \cdot a \cdot \left(P_{C_3H_8} - \dfrac{P_{C_3H_6} \cdot P_{H_2}}{K_1} \right)}{1 + K_2 \cdot P_{C_3H_6}}$$

$$3CH_{0.5} + 3.25\,H_2$$

$$C_C = C_{C\max} \cdot \frac{k_2 - k_3}{k_2} \cdot (1 - e^{-k_1 \cdot t}) + k_3 \cdot C_{C\max} \cdot t$$

$$a = \exp(-\alpha_1 \cdot C_m) \cdot \exp(-\alpha_2 \cdot C_M)$$

Butane partial oxidation to maleic anhydride

$$(-r_1) = k_1 \cdot P_{O_2} \cdot (1 - \lambda_O)$$

$$(-r_{-1}) = k_{-1} \cdot \lambda_O$$

$$(-r_2) = k_2 \cdot \lambda_O \cdot (1 - \theta_{surface})$$

$$(-r_3) = k_3 \cdot (\theta_{subsurface} - \theta_{surface})$$

$$(-r_4) = k_4 \cdot P_{C_4H_{10}} \lambda_O$$

$$(-r_5) = k_5 \cdot P_{C_4H_{10}} \lambda_O^2$$

$$(-r_6) = \frac{k_6 \cdot P_{C_4H_{10}} \theta_{surface}^2}{1 + K_{eq_2} \cdot P_{C_4H_{10}} + K_{eq_1} P_{O_2}}$$

$$(-r_7) = \frac{k_7 \cdot P_{C_4H_{10}} \theta_{surface}}{1 + K_{eq_2} \cdot P_{C_4H_{10}} + K_{eq_1} P_{O_2}}$$

$$(-r_8) = \frac{k_8 \cdot P_{C_4H_{10}} \theta_{surface}}{1 + K_{eq_2} \cdot P_{C_4H_{10}} + K_{eq_1} P_{O_2}}$$

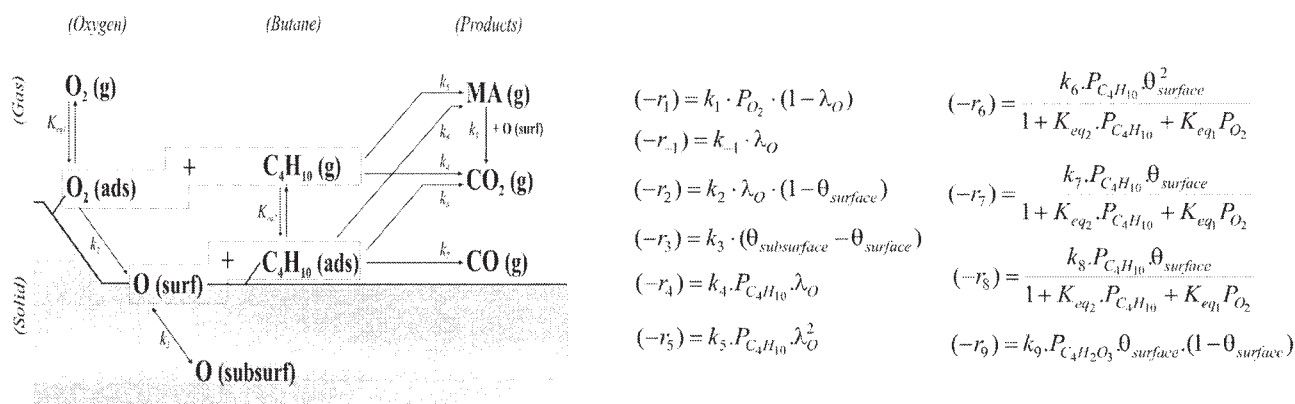$$(-r_9) = k_9 \cdot P_{C_4H_2O_3} \theta_{surface} \cdot (1 - \theta_{surface})$$

Figure 2. Kinetics used in this work for the dehydrogenation of propane and the partial oxidation of n-butane.

ene). Coke formation kinetics correspond to a monolayer–multilayer mechanism, while the influence of coke content over the catalyst activity is given by an exponential equation that takes into account monolayer and multilayer coke growth. The values of the kinetic constants are given in Table 2.

Table 2. Kinetic Data Used in This Work for the Dehydrogenation of Propane (Figure 2a)

Parameter [units]	Value
k_{01} [mmol/g · s · bar]	5.16 E-2
K_{02} [−]	3450
E_{a1} [kJ/mol]	35.5
ΔH [kJ/mol]	−595
α_1 [g · cat/g · coke]	813
α_2 [g · cat/g · coke]	289
k_{02} [s^{-1}]	2.42 E-3
k_{03} [s^{-1}]	3.57 E-4
E_{a2} [kJ/mol]	221
E_{a3} [kJ/mol]	325.8
$C_{\max}$ [mg coke/mg cat]	6.82 E-4
k_{04} [mmol/g · s · bar]	1 E-4
E_{a4} [kJ/mol]	308

Arrhenius type dependency was assumed and parameters are reparametrized according to: $k_i = k_{0i} \cdot \exp - Ea_i \cdot (1/T - 1/T_m))$ or $K_i = K_{0i} \cdot \exp(-\Delta H \cdot (1/T - 1/T_m))$, with $T_m = 823$ K.

Butane Partial Oxidation to Maleic Anhydride. The kinetics of butane partial oxidation to maleic anhydride over a VPO catalyst has recently been studied in detail.[17] The proposed model (Figure 2b) assumes the presence of adsorbed oxygen in the catalyst and catalyst's oxygen (surface and subsurface). Adsorbed oxygen reacts with n-butane to produce COx and maleic anhydride. In addition, the oxygen in the superficial layers of the catalyst is consumed in the oxidation reactions to maleic anhydride and COx (mainly CO), being replenished by diffusion from the subsurface. Reactions take place between the surface oxygen and the adsorbed n-butane, which adsorbs in different sites than adsorbed oxygen. When the catalyst is reoxidized, oxygen in the gas phase reacts to form adsorbed oxygen, then is incorporated in the superficial layers, and finally diffuses from the surface to the subsurface. The values of the kinetic constants are given in Table 3.

Mass Balances

The reactor model considers nine gaseous compounds for the propane dehydrogenation: argon, propane, propene, methane, ethylene, water, hydrogen, oxygen, and CO_2. For the partial oxidation of n-butane, seven gaseous compounds are considered: helium, oxygen, n-butane, maleic anhydride, CO_2, CO, and water. Mass balances for the gas phase are similar for both

Table 3. Kinetic Data Used in This Work for the Partial Oxidation of n-Butane (Figure 2b)

Parameter [units]	Value	Parameter [units]	Value
k_{01} [mmol/min $\cdot$ g $\cdot$ bar]	9.820	k_{07} [mmol/min $\cdot$ g $\cdot$ bar]	0.489
Ea_1 [kJ/mol]	33.1	Ea_7 [kJ/mol]	106.1
k_{02} [mmol/min $\cdot$ g]	0.331	k_{08} [mmol/min $\cdot$ g $\cdot$ bar]	0.166
Ea_2 [kJ/mol]	30.9	Ea_8 [kJ/mol]	82.0
k_{03} [mmol/min $\cdot$ g]	0.219	k_{09} [mmol/min $\cdot$ g $\cdot$ bar]	0.087
Ea_3 [kJ/mol]	134.0	Ea_9 [kJ/mol]	137.9
k_{04} [mmol/min $\cdot$ g $\cdot$ bar]	0.140	K_{0eq1} [bar^{-1}]	55.85
Ea_4 [kJ/mol]	138.1	ΔH_1 [kJ/mol]	-30.6
k_{05} [mmol/min $\cdot$ g $\cdot$ bar]	0.855	K_{0eq2} [bar^{-1}]	94.213
Ea_5 [kJ/mol]	50.3	ΔH_2 [kJ/mol]	-114.3
k_{06} [mmol/min $\cdot$ g $\cdot$ bar]	0.349	N_S [mgO/g]	2.44
Ea_6 [kJ/mol]	32.4	N_L [mgO/g]	11.6

Arrhenius type dependency was assumed and parameters are reparametrized according to: $k_i = k_{0i} \cdot \exp - Ea_i \cdot (1/T - 1/T_m))$ or $K_i = K_{0i} \cdot \exp(-\Delta H \cdot (1/T - 1/T_m))$, with $T_m = 673$ K.

kinds of reactor (the flow for the gas is the same independent of the shape of the fluidized bed) and for both reactions (the only difference is in the kinetics). They are as follows:

In the bubble and wake phase:

$$\frac{\partial((\alpha + f_w \cdot \alpha \cdot \varepsilon_{mf}) \cdot A \cdot C_{i,B})}{\partial t}$$
$$= \frac{-\partial((\alpha + \alpha \cdot f_w \cdot \varepsilon_{mf}) \cdot A \cdot u_B \cdot C_{i,B})}{\partial z}$$
$$+ (\lambda_1 \cdot C_{i,B} + \lambda_2 \cdot C_{i,e}) \cdot \frac{\partial((\alpha + \alpha \cdot f_w \cdot \varepsilon_{mf}) \cdot A \cdot u_B)}{\partial z}$$
$$- K_{B,e} \cdot A \cdot (\alpha + \alpha \cdot f_w \cdot \varepsilon_{mf}) \cdot (C_{i,B} - C_{i,e})$$
$$+ r_{i,B} \cdot \rho \cdot \frac{(1 - \varepsilon_{mf}) \cdot f_w}{(1 + f_w \cdot \varepsilon_{mf})} \cdot A \cdot (\alpha + f_w \cdot \alpha \cdot \varepsilon_{mf}) \quad (1)$$

In the emulsion phase:

$$\frac{\partial((1 - (\alpha + \alpha \cdot f_w)) \cdot A \cdot C_{i,e})}{\partial t}$$
$$= \frac{-\partial(A \cdot (1 - (\alpha + \alpha \cdot f_w)) \cdot u_{mf} \cdot C_{i,e})}{\partial z}$$
$$- (\lambda_1 \cdot C_{i,B} + \lambda_2 \cdot C_{i,e}) \cdot \frac{\partial((\alpha + \alpha \cdot f_w \cdot \varepsilon_{mf}) \cdot A \cdot u_B)}{\partial z}$$
$$- K_{B,e} \cdot A \cdot (\alpha + \alpha \cdot f_w \cdot \varepsilon_{mf}) \cdot (C_{i,e} - C_{i,B})$$
$$+ r_{i,B} \cdot \rho \cdot (1 - \varepsilon_{mf}) \cdot A \cdot (1 - (\alpha + f_w \cdot \alpha \cdot \varepsilon_{mf})) \quad (2)$$

The flow model for the solid is different depending on the reactor and on the reaction kinetics, as has been explained above. For the dehydrogenation of propane, the main variable concerning the solid is the amount of coke over its surface (coke concentration), which will vary along the bed but will remain almost constant in the steady state. Regarding the partial oxidation of n-butane, since two different oxygen concentrations of the catalyst have been taken into account in the kinetic model (Figure 2), two terms will appear in the reactor model for the solid mass balances in wake and emulsion. The detailed equations for each reactor and reaction system are shown below.

Propane dehydrogenation:
In the wake: TZFBR and ICFBR

$$\frac{A \cdot f_w \cdot \rho \cdot \partial(\alpha \cdot C_{c,w})}{\partial t} = -\frac{A \cdot \rho \cdot f_w \cdot \partial(\alpha \cdot u_B \cdot C_{c,w})}{\partial z}$$
$$+ (\lambda_1 \cdot C_{c,w} + \lambda_2 \cdot C_{c,e}) \cdot \frac{A \cdot f_w \cdot \partial(\alpha \cdot u_B)}{\partial z}$$
$$- K_{w,e} \cdot A \cdot f_w \cdot \alpha \cdot \rho \cdot (C_{c,w} - C_{c,e}) + r_{C_c} \cdot f_w \cdot \alpha \cdot A \cdot \rho \quad (3)$$

In the emulsion
TZFBR:

$$\frac{A \cdot \rho \cdot \partial((1 - \alpha - \alpha \cdot f_w) \cdot C_{c,e})}{\partial t}$$
$$= -\frac{A \cdot \rho \cdot \partial((1 - \alpha - \alpha \cdot f_w) \cdot u_{s,e} \cdot C_{c,e})}{\partial z}$$
$$- (\lambda_1 \cdot C_{c,w} + \lambda_2 \cdot C_{c,e}) \cdot \frac{A \cdot f_w \cdot \partial(\alpha \cdot u_B)}{\partial z}$$
$$- K_{e,w} \cdot A \cdot (1 - \alpha - \alpha \cdot f_w) \cdot \rho \cdot (C_{c,e} - C_{c,w})$$
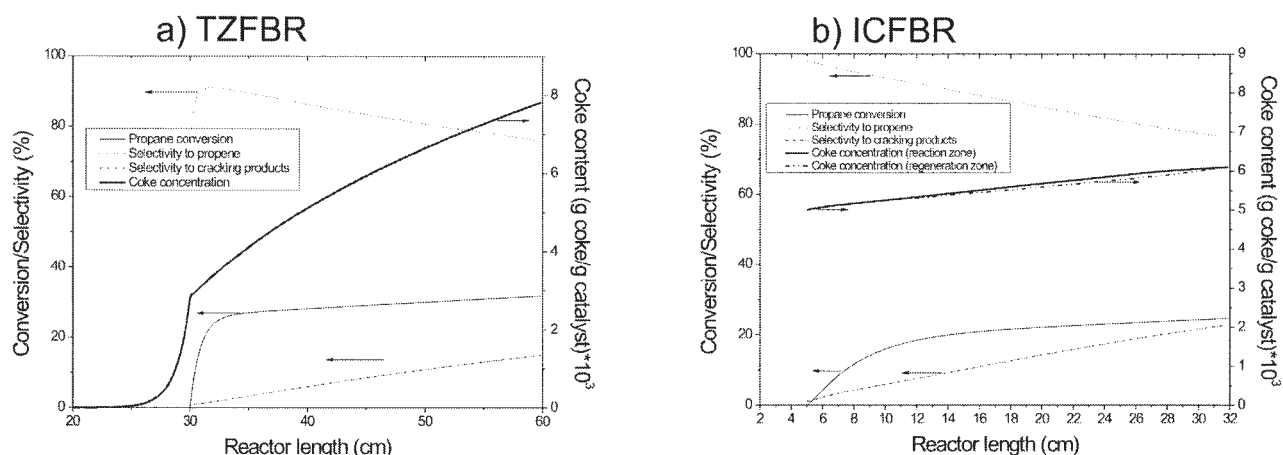$$+ r_{C_c} \cdot (1 - \alpha - \alpha \cdot f_w) \cdot A \cdot \rho \quad (4)$$

ICFBR:

$$\frac{A \cdot \rho \cdot \partial((1 - \alpha - \alpha \cdot f_w) \cdot C_{c,e})}{\partial t}$$
$$= -\frac{\partial((1 - \alpha - \alpha \cdot f_w) \cdot G_{s,e} \cdot C_{c,e})}{\partial z}$$
$$- (\lambda_1 \cdot C_{c,w} + \lambda_2 \cdot C_{c,e}) \cdot \frac{A \cdot f_w \cdot \partial(\alpha \cdot u_B)}{\partial z}$$
$$- K_{e,w} \cdot A \cdot (1 - \alpha - \alpha \cdot f_w) \cdot \rho \cdot (C_{c,e} - C_{c,w})$$
$$+ r_{C_c} \cdot (1 - \alpha - \alpha \cdot f_w) \cdot A \cdot \rho \quad (5)$$

Butane oxidation:
In the wake: TZFBR and ICFBR

Figure 3. Model predictions for the evolution of propane conversion, selectivity to propene, selectivity to cracking products, and coke profiles along the bed for both reactor configurations used in the propane catalytic dehydrogenation.

T = 550 °C; W/F = 100 g.h/mol; Q_{Ar} = 18 cm³ (STP)/s; Q_{C3H8} = 26 cm³(STP)/s; Q_{O2} = 2 cm³(STP)/s; h_b/h_0 = 0.5 (TZFBR); u_r = 3.

$$\frac{A \cdot f_w \cdot \rho \cdot \partial(\alpha \cdot \theta_{i,w})}{\partial t} = -\frac{A \cdot \rho \cdot f_w \cdot \partial(\alpha \cdot u_B \cdot \theta_{i,w})}{\partial z}$$

$$+ (\lambda_1 \cdot \theta_{i,w} + \lambda_2 \cdot \theta_{i,e}) \cdot \frac{A \cdot f_w \cdot \partial(\alpha \cdot u_B)}{\partial z}$$

$$- K_{w,e} \cdot A \cdot f_w \cdot \alpha \cdot \rho \cdot (\theta_{i,w} - \theta_{i,e}) + r_{C_c} \cdot f_w \cdot \alpha \cdot A \cdot \rho \quad (6)$$

In the emulsion
TZFBR:

$$\frac{A \cdot \rho \cdot \partial((1 - \alpha - \alpha \cdot f_w) \cdot \theta_{i,e})}{\partial t}$$

$$= -\frac{A \cdot \rho \cdot \partial((1 - \alpha - \alpha \cdot f_w) \cdot u_{s,e} \cdot \theta_{i,e})}{\partial z} - (\lambda_1 \cdot \theta_{i,w} + \lambda_2 \cdot \theta_{i,e})$$

$$\cdot \frac{A \cdot f_w \cdot \partial(\alpha \cdot u_B)}{\partial z} - K_{e,w} \cdot A \cdot (1 - \alpha - \alpha \cdot f_w) \cdot \rho \cdot (\theta_{i,e} - \theta_{i,w})$$

$$+ r_{C_c} \cdot (1 - \alpha - \alpha \cdot f_w) \cdot A \cdot \rho \quad (7)$$

ICFBR:

$$\frac{A \cdot \rho \cdot \partial((1 - \alpha - \alpha \cdot f_w) \cdot \theta_{i,e})}{\partial t}$$

$$= -\frac{\partial((1 - \alpha - \alpha \cdot f_w) \cdot G_{s,e} \cdot \theta_{i,e})}{\partial z}$$

$$- (\lambda_1 \cdot \theta_{i,w} + \lambda_2 \cdot \theta_{i,e}) \cdot \frac{A \cdot f_w \cdot \partial(\alpha \cdot u_B)}{\partial z}$$

$$- K_{e,w} \cdot A \cdot (1 - \alpha - \alpha \cdot f_w) \cdot \rho \cdot (\theta_{i,e} - \theta_{i,w})$$

$$+ r_{C_c} \cdot (1 - \alpha - \alpha \cdot f_w) \cdot A \cdot \rho \quad (8)$$

The term $\partial(u_B \cdot \alpha)/\partial z \cdot (\lambda_1 \cdot C_{i,B} + \lambda_2 \cdot C_{i,e})$ [31-33] takes into account the solid flow between wake and emulsion as a consequence of the variation of the bubble properties with

height. A change in the volume of the bubble must be compensated by a net gas (or solid) flow from the emulsion to the bubble and wake or vice-versa. This is done as follows:

$$\lambda_1 = 1 \quad \lambda_2 = 0 \quad \text{when } \frac{\partial(u_B \cdot \alpha)}{\partial z} < 0 \quad (9a)$$

$$\lambda_1 = 0 \quad \lambda_2 = 1 \quad \text{when } \frac{\partial(u_B \cdot \alpha)}{\partial z} \geq 0 \quad (9b)$$

The mass balances for each case constitute a system of partial differential equations. In steady state the derivatives with respect to time are null, resulting in an ODE system that is solved by applying a solver based on the numerical differentiation formulas[34,35] specially recommended for stiff problems. Solution in the steady state has been searched for in each of the four reactor models. In the case of TZFBR, the process applied consisted in the search (by a simplex method) for a value of the concentration of coke (for propane dehydrogenation) or of the surface and lattice oxidation state of the catalyst (for n-butane partial oxidation) in the bottom part of the reactor that would close the mass balance of oxygen. In the case of ICFBR, this search is aimed at closing the mass balance of oxygen and forecasting the same concentration of coke (for propane dehydrogenation) or the same catalyst oxidation states (for the selective oxidation) at the top and the bottom part of each interconnected reactor.

Results and Discussion

The models described above have been employed to predict the performance of the TZFBR and ICFBR, as well as to provide an estimate of the concentration profiles of the different species in the gas and solid phase along the different reactors. The methods developed could be employed in further optimization, as well as to devise improved operation methods.
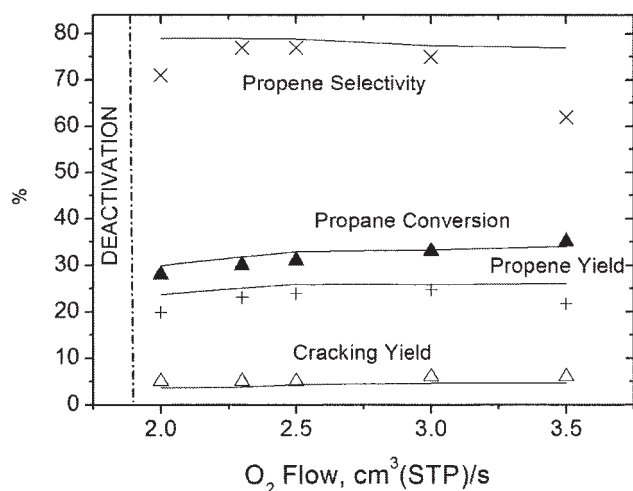
Figure 4. Influence of the O_2 flow upon propane conversion, propene selectivity, and cracking yield.

Experimental data (symbols) versus model prediction (lines). Configuration: TZFBR; T = 550°C; W/F = 150 g.h/mol; Q_{Ar} = 24 cm³ (STP)/s; Q_{C3H8} = 26 cm³ (STP)/s; h_b/h_0 = 0.5; u_r = 3.6.

Dehydrogenation of propane

Figure 3 shows the model prediction for the variation of conversion, selectivity to propene, selectivity to cracking products, and coke profiles along the bed for both reactor configurations. Since propane dehydrogenation is an equilibrium limited reaction, conversion rise decreases dramatically when closing the equilibrium conversion (35% approximately at 550°C). Low selectivities to propene in the bottom part of the reaction zone of the TZFBR (Figure 3a) are due to the combustion of propane with the oxygen not converted in the regeneration zone. The fast increase of the coke concentration in the last part of the regeneration zone for the TZFBR is produced by the sum of two facts: the decrease in the oxygen partial pressure and the nearness to the reaction zone. The evolution of the coke profile in the ICFBR (Figure 3b) is also remarkable; the amount of coke in the reaction zone is smaller than that of the TZFBR. Since coke growth depends only on the time,[16] we can conclude that the residence time for the catalyst in each zone is smaller in the ICFBR.

The amount of O_2 fed turned out to be one of the most important variables in our previous experimental work.[1] Figure 4 shows its effect for a set of experiments performed with a constant input of argon and propane and different O_2 inputs. The model predictions are in agreement with the observed experimental trend (a maximum in propene yield is found for an intermediate O_2 flow). As has been pointed out, too small amounts of oxygen are not able to regenerate the catalyst, producing a decrease in conversion, while an excess of oxygen will react with the propane when reaching the reaction zone, resulting in a selectivity decrease.

Figure 5 shows a comparison between the model predictions of coke profiles along the bed with the experimental data obtained by analyzing catalyst samples gathered from the reactor after 8 hours under steady state conditions. The predictions agree more than satisfactorily taking into account the difficulty in obtaining reliable experimental data (catalyst samples were obtained with the help of a solid probe).

The comparison between the model prediction for the experiment with 2 cm³ (STP)/s of oxygen with the prediction shown in Figure 3a is also very interesting: the experimental conditions are similar, the only difference being the amount of argon fed. This is greater in the Figure 5 experiment, which corresponds with the smallest amount of coke (although the oxygen concentration in the regeneration zone is greater for the smallest amount of inert gas). This fact shows again the great influence of the catalyst circulation between both zones. On the other hand, propane conversion is almost the same for both experiments. Although the bubble diameter increases with an increase in the gas flow, this is because of the sum of two facts: the equilibrium conversion increases with increasing propane dilution and the amount of coke is smaller, and therefore the activity of the catalyst is greater.

The influence of the catalyst circulation on the performance is more remarkable in the ICFBR system. Figure 6 shows the fit of the experimental and model prediction for propene yield against the predicted velocity of catalyst circulation for three sets of experiments with the same flowrate of propane fed in zone 2 (Figure 1b), and three different oxygen flowrates, fed in zone 3 (Figure 1b). Differences in catalyst circulation were obtained by feeding different inert amounts with the propane, thus increasing the porosity in the reaction zone but keeping the porosity constant in the regeneration zone. From the plot, it can be deduced that, in the case of the ICFBR, an increase in the amount of oxygen fed should always be advantageous because oxygen will never reach the reaction zone (the zones are separated by a vertical plate instead of relying on the oxygen consumption, as in the TZFBR) The largest discrepancy between the model predictions and the experimental data is found in the high solid interchange velocity zone: as is shown in Figure 6, experiments with the smallest amounts of oxygen (1 and 1.5 cm³(STP)/s) produce experimental results better than those forecast by the reactor model, while experimental yields for the experiments with the highest amount of oxygen are lower than the predictions of the model. This trend can be related with the capability of Cr_2O_3/Al_2O_3 catalyst to promote combustion.[36,37] This fact was not taken into account in the
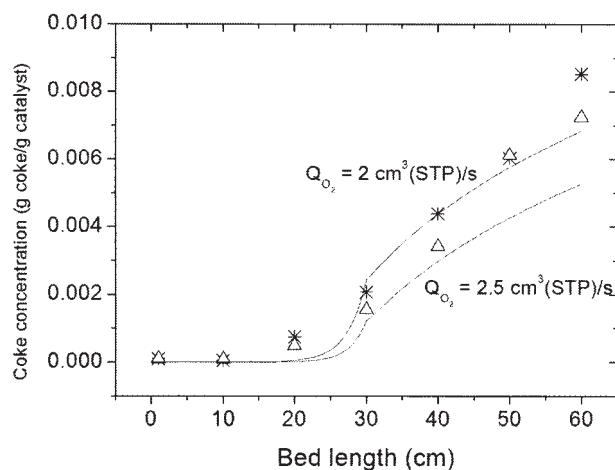
Figure 5. Coke concentration along the catalyst bed for two different O_2 flowrates fed into the reactor.

Experimental data (symbols) versus model prediction (lines). Same operation conditions as in Figure 4.
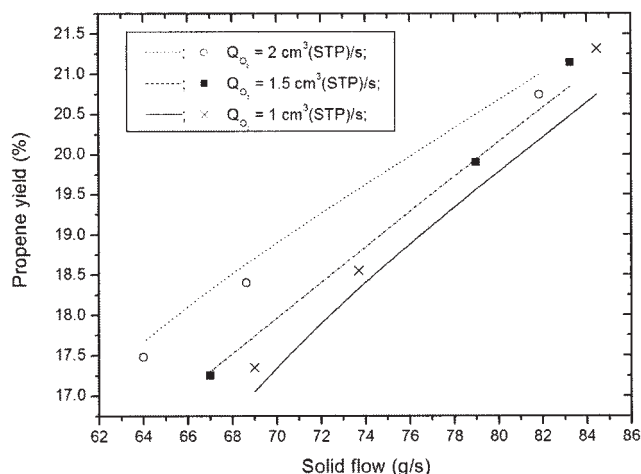
Figure 6. Effect of the velocity of solid interchange between zones in the ICFBR reactor over propene yield.

Experimental data (symbols) vs. model prediction (lines). T = 550°C; W/F = 100 g.h/mol; Q_{Ar1} (bottom part of the reactor) = 16 cm³ (STP)/s; Q_{C3H8} = 26 cm³ (STP)/s; Q_{Ar2} (mixed with the propane) = 5-16 cm³ (STP)/s; Q_{O2} = 1-2 cm³ (STP)/s.

kinetic model and, therefore, the reactor model will not be able to forecast this behavior.

Figure 7 shows a comparison between the experimental data and model predictions for the effect of the temperature upon propane conversion and propene selectivity for a set of experiments carried out in the TZFBR with a constant input of propane and argon, while the flow of oxygen was varied to achieve an optimum steady state at each temperature. As might be expected from the kinetic model, selectivity to propene
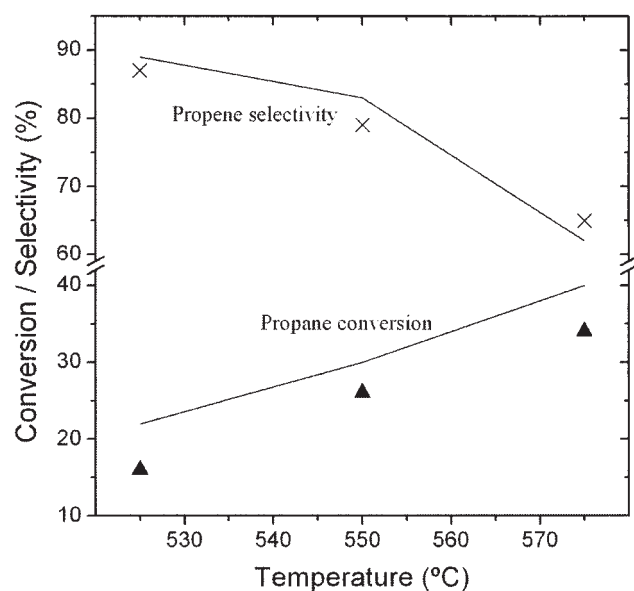
Figure 7. Effect of temperature upon propane conversion and propene selectivity.

Experimental data (symbols) vs. model prediction (lines). Configuration: TZFBR; W/F = 125 g.h/mol; Q_{Ar} = 24 cm³ (STP)/s; Q_{C3H8} = 26 cm³ (STP)/s; h_b/h_0 = 0.5; u_r = 3.6.
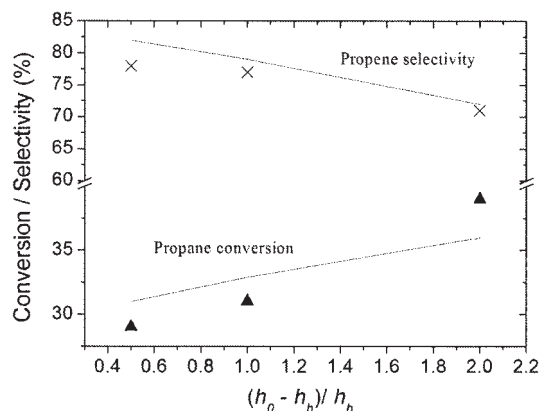
Figure 8. Influence of relation between the length of the reducing and the oxidizing zones using the same amount of catalyst in the bed.

Experimental data (symbols) vs. model prediction (lines). Configuration: TZFBR; T = 550°C; Q_{Ar} = 24 cm³ (STP)/s; Q_{C3H8} = 26 cm³ (STP)/s; Q_{O2} = 2.5 cm³ (STP)/s; W = 800 g; u_r = 3.6.

decreases dramatically by increasing the temperature as a result of the difference between the activation energies of propane dehydrogenation and the cracking reaction (the second is 10 times larger than the first) and the strong effect of temperature upon coke formation.

The relative size of each zone for the TZFBR has also been studied. Figure 8 shows the propane conversion and selectivity to propene for three experiments with the same catalyst weight loaded in the reactor but with different propane entry points, that is, for the same total height of the bed (H) but differences between the height of the reducing and the oxidizing zones (thus, different W_r/F ratios). The feed flows of oxygen, propane, and argon in the reactor were the same for each case. The experimental trend of increasing conversion and decreasing selectivity with increasing the reaction/regeneration zone height ratio is confirmed by the reactor model. Coke content in the reaction zone increases by decreasing this ratio, which results in a less selective catalyst.

Partial oxidation of n-butane to maleic anhydride

Figure 9 shows the model prediction for the variation of conversion, selectivity to maleic anhydride, selectivity to CO_x, and profiles of internal lattice and surface lattice oxygen along the bed for both reactor configurations. The evolution of the oxygen content in the catalyst is very remarkable: consumption of oxygen in the catalyst core (named lattice oxygen) is diffusion controlled in both reactors, either in the presence or absence of oxygen in the gas phase, while the consumption of adsorbed oxygen changes depending on the presence or absence of gas phase oxygen in the reaction zone. In the case of the TZFBR, some gas phase oxygen remaining from the regeneration zone (at the bottom part of the reactor) reaches the top part, maintaining the adsorbed oxygen over the catalyst. On the other hand, in the case of the ICFBR plotted experiment, no gas phase oxygen is present in the reaction zone, which produces fast adsorbed oxygen consumption. Since the catalyst oxidation state profile in each reactor is different, a different conversion–selectivity curve is obtained for each reaction prod-

a) TZFBR

b) ICFBR
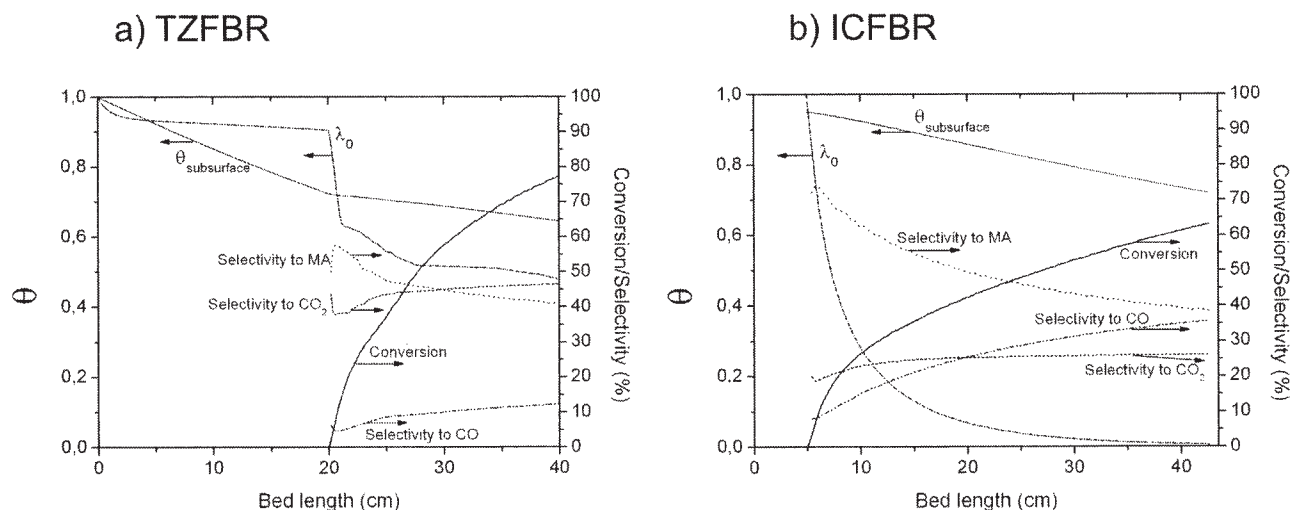
Figure 9. Evolution of n-butane conversion, selectivity to maleic anhydride, selectivity to CO and CO$_2$, and θ and λ profiles along the bed for both reactor configurations used in the partial oxidation of n-butane.
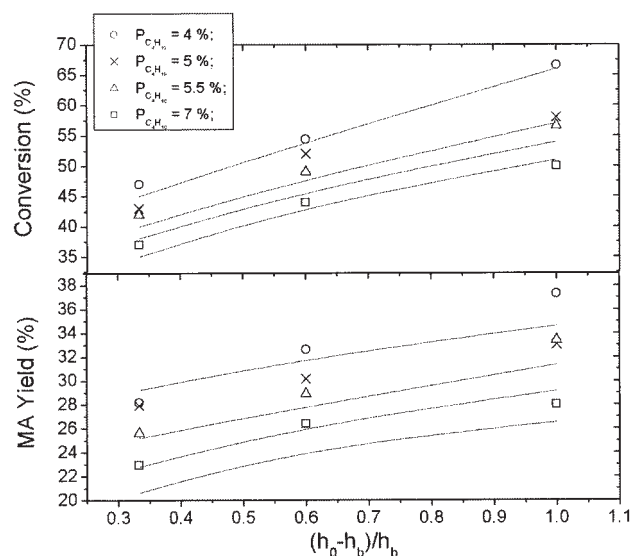
Experimental data (symbols) vs. model prediction (lines). T = 420°C; P$_{C4H10}$ = 4%; P$_{O2}$ = 24%; u$_r$ = 3; TZFBR i.d. = 6 cm; h$_0$ = 40cm; h$_b$/h$_0$ = 0.5; ICFBR i.d. = 10cm.

uct, that is, selectivity to CO is greater than CO$_2$ selectivity in the case of the ICFBR (gas phase oxygen absence), while in the TZFBR CO$_2$ is 4 times greater than CO selectivity. On the other hand, MA selectivity follows similar behavior in both reactor configurations: when the n-butane comes into contact with the highly oxidized catalyst, complete oxidation to CO$_2$ is the main occurring reaction, producing low MA selectivity. When the catalyst surface is not totally oxidized ($\lambda_0 \sim 0.8$), a maximum in MA selectivity appears, decreasing after this point. The difference between the reactors is a result of the gas phase oxygen present in the TZFBR, which replenishes the catalyst oxygen. These trends are in agreement with the experimental results obtained in the TZFBR and ICFBR,[2] as well as with several studies.[38] It is important to note at this point that since an intermediate catalyst oxidation state is necessary for achieving the best results, the velocity of the solid circulation will also play a key role in this reaction.

The influence of the relative size of each zone for the TZFBR has also been studied; Figure 10 shows the effect of this variable on butane conversion and MA yield for a set of experiments under different n-butane partial pressures with the same catalyst weight loaded in the reactor but with different propane entry points. As expected, the n-butane conversion increases when the reaction zone increases, but increases in the MA yield are almost negligible. This fact is explained by the model as a result of the degree of catalyst reduction, which increases when increasing either the n-butane partial pressure or the reaction zone length.

Another interesting trend is the existence of an optimum n-butane–oxygen ratio to be fed into the reactor in order to achieve a maximum MA yield. This trend, observed experimentally, has been compared with the predictions of the model. Figure 11 shows the experimental data with the model predictions for n-butane conversion and MA selectivity as well as model predictions for O$_2$ pressure and catalyst oxygen evolution along the bed for a set of experiments where, maintaining the n-butane pressure and the total gas flow constant, the

O$_2$/n-butane ratio was varied between 4 and 8. As is shown, the best selectivity results are obtained for an O$_2$/n-butane ratio of around 6. Values in the reaction zone of $\lambda_0 \sim 0.6$ and $\theta_{subsurface} \sim 0.8$ seem to be the most appropriate for performing the partial oxidation of n-butane at this temperature (400°C), which agrees with several authors.[39] This very interesting fact suggests that there should exist an optimal O$_2$/n-butane ratio for each n-butane concentration and n-butane entry point and for each temperature. Furthermore, it also provides a driving force for developing new reactor configurations, such as mem-

Figure 10. Influence of relation between the length of the reducing and the oxidizing zones using the same amount of catalyst in the bed.

Experimental data (symbols) vs. model prediction (lines). Configuration: TZFBR; T = 400°C; P$_{O2}$/P$_{C4H10}$= 6; Q$_T$ = 2600 cm^3 (STP)/s; W = 600 g; u$_r$ = 3.
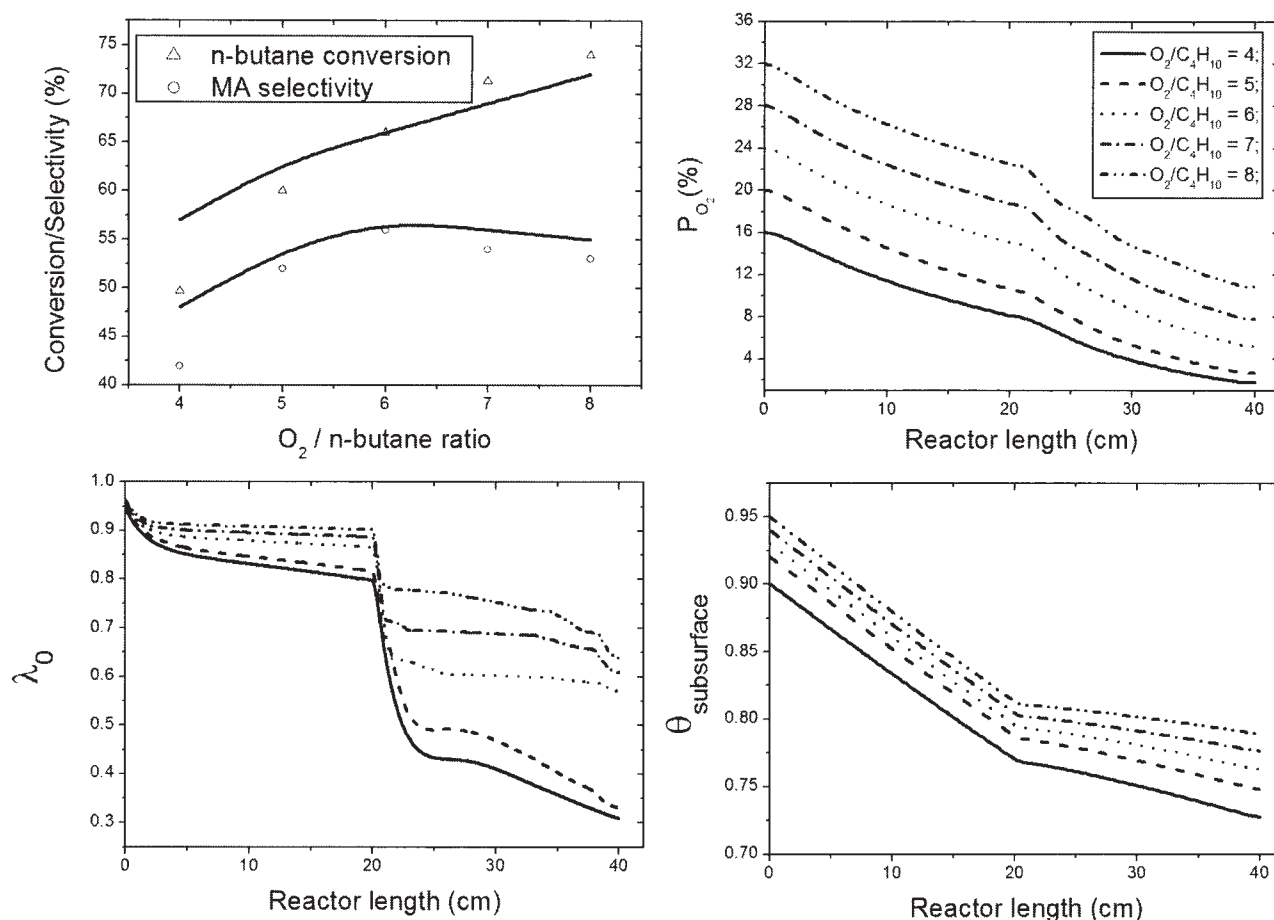
Figure 11. Influence of the O_2/n-butane ratio on n-butane conversion, MA selectivity and oxygen content profiles in the bed.

(a) Experimental data (symbols) vs. model prediction (lines). (b) Model predictions for the evolution of oxygen partial pressure. (c) and (d) Model predictions for the evolution of oxygen content in the catalyst. Configuration: TZFBR. T = 400°C; P_{C4H10} = 4%; Q_T = 2600 cm^3 (STP)/s; h_0 = 40cm; h_b/h_0 = 0.5; W = 600 g; u_r = 3.

brane reactors,[40,41] where the distribution of O_2 is almost constant along the catalyst bed, or CFB reactors,[9] where the small residence time of the catalyst (which can be varied by controlling the solid flow between both catalyst beds) in the reaction zone also allows a good control of the oxidation state of the catalyst.
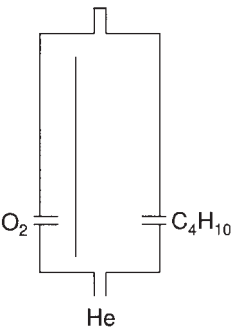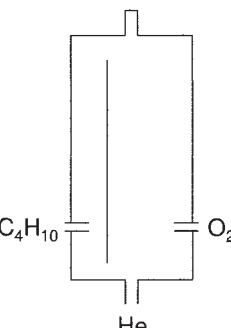
In order to gain a better insight into the effect of the residence time, two sets of experiments were performed in the ICFBR system: in each of them, butane was fed to a different reactor compartment, that is, the axial slot allows the partition of the reactor vessel into two beds of different sizes, interconnected at the bottom and the top, and in this study butane was fed in some experiments to the smallest bed and in other cases to the largest bed, while a He-O_2 mixture was fed to the opposite bed. Table 4 shows the experimental results for n-butane conversion and maleic anhydride selectivity together with the model predictions for the average oxidation states of the catalyst in each case. As expected, the oxidation state of the catalyst in the bed is higher in the experiments with the shortest catalyst residence time (configuration 2), resulting in a better reactor performance. Considering these results, it would be expected that feeding some oxygen together with the n-butane in the reaction zone of the ICFBR should increase the maleic

anhydride selectivity. Figure 12 shows the variation of conversion and MA yield for a set of experiments where different amounts of oxygen were added together with the n-butane flow, while the total flow of oxygen was kept constant, maintaining an O_2/n-butane ratio of 6. As is shown, the effect of adding some gaseous oxygen together with the n-butane is beneficial for the performance of the reactor.

Final Considerations About the Model

In simulation studies in general, a balance must be struck between model applicability, the time necessary to reach a solution, and reliability of the forecast data. Obviously, the best model will be that able to be applied to the majority of conditions in the shortest possible time. In the first model for a TZFBR presented by our group,[15] a parametric study of the effect of the bubble diameter over the main reactor-related variables demonstrated that when using a lab scale reactor, this variable has little effect on the performance. In the present work, involving the attempted simulation of experiments at bench scale, it has been necessary to add a varying bubble diameter to the model. This has necessitated the inclusion of new terms in the mass balances, resulting in a more compli-

Table 4. Influence of the Relative Size for Oxidizing and Reducing Zones in the ICFBR Reactor

	% n-Butane	X (experimental)/X (model)	S_{MA} (exp)/S_{MA} (model)	θ_{ads}	$\theta_{lattice}$
Configuration 1 (O₂ / C₄H₁₀ / He)	4	68/70	43/38	0.12	0.83
	5	65/63	43/38	0.09	0.81
	6	61/59	43/39	0.06	0.79
	7	57/54	44/42	0.047	0.78
	8	50/49	47/42	0.038	0.76
	% n-Butane	X (experimental)/X (model)	S_{MA} (exp)/S_{MA} (model)	θ_{ads}	$\theta_{lattice}$
Configuration 2 (C₄H₁₀ / O₂ / He)	4	75/75	47/52	0.28	0.93
	5	69/66	50/51	0.23	0.91
	6	55/55	52/50	0.18	0.90
	7	43/46	53/48	0.15	0.90
	8	41/38	52/46	0.12	0.90

$W = 1500$ g, $F_t = 6600$ cm³ (STP)/min.

cated and slower to solve mathematical problem, especially because of the addition of the transversal flow term. This term makes the model more unstable from a mathematic point of view; furthermore, achieving a solution for the differential equations system proposed in the mass balances requires more computational resources. In these circumstances, it should be questioned whether this improvement is worthwhile or if it only results in using up computational resources without a corresponding improvement in the performance of the model. To this end, we have compared the results forecast by models
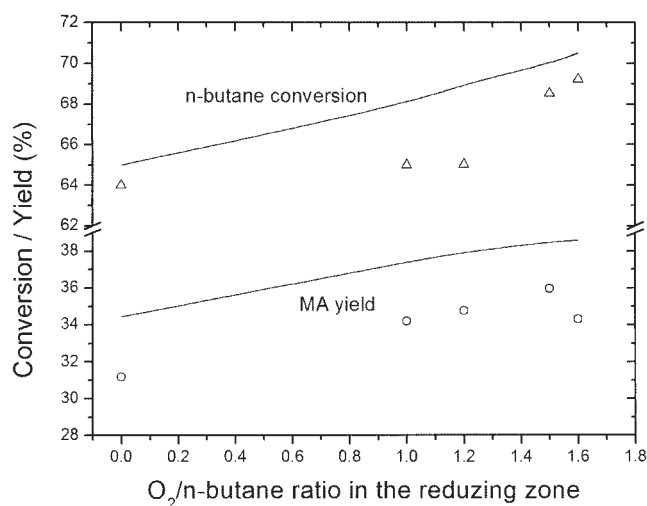
Figure 12. Effect of the presence of gas phase oxygen in the reducing zone in the ICFBR.

Experimental data (symbols) vs. model prediction (lines). $C_{C4H10} = 4\%$; $T = 400°C$.
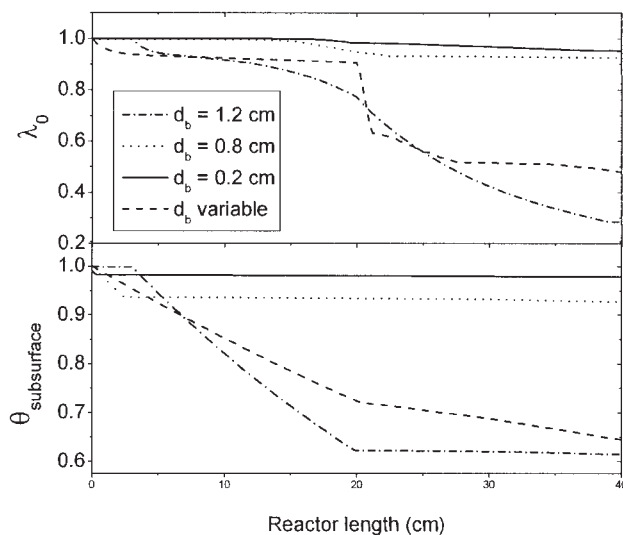
Figure 13. Influence of the bubble diameter on the oxygen adsorbed and catalyst oxygen in the TZFBR reactor (maleic anhydride synthesis).

$T = 420°C$; $P_{C4H10} = 4\%$; $P_{O2} = 24\%$; $u_r = 3$; $h_0 = 40$cm; $h_b/h_0 = 0.5$.

Table 5. Influence of the Bubble Diameter in the Performance of the Mathematical Model in the TZFBR Reactor (maleic anhydride synthesis)

	Bubble Diameter	n-Butane Conversion (%)	MA Selectivity (%)
Experimental	—	71	41
Constant d_b	0.2 cm	92	39
Constant d_b	0.8 cm	81	40
Constant d_b	1.2 cm	65	35
d_b Variable	0.1-1.3 cm	73	41

$T = 420°C$; $P_{C4H10} = 4\%$; $P_{O2} = 24\%$; $u_r = 3$; $h_0 = 40$ cm; $h_b/h_0 = 0.5$.

both with and without a constant bubble diameter for the partial oxidation of n-butane in a TZFBR. For this reactor, the forecast bubble diameter[26] varies between 0.1 and 1.3 cm. Diameters of 0.2, 0.8, and 1.4 cm have been tested in the model with a constant d_b.

Figure 13 shows the variation of the surface and lattice oxygen calculated with the model using either a constant d_b or variable d_b for some given experimental conditions. Table 5 shows the forecast n-butane conversion and MA selectivity as well as the experimentally observed conversion and selectivity for the given conditions. As can be observed, several differences exist between each prediction. A small bubble diameter produces a fast reaction rate and little solid circulation,[15] while gas phase oxygen oxidizes the catalyst quickly, producing almost constant profiles in the whole reactor. A large bubble diameter means that a large part of the gas in the bubble crosses the bed without contacting the catalyst, and the circulation of solids is greater. Gas phase oxygen is not able to oxidize the catalyst, resulting in a poorer reactor performance. On the other hand, the use of a model with a variable bubble diameter provides better results: the forecast conversion and selectivity are close to experimental data (Table 5), and more coherent predictions for the catalyst oxidation state are given.

This study leads to the conclusion that the bubble diameter has a large effect on the model performance when exceeding the lab scale. Although the inclusion of new terms in the mass balances could slow down the process of reaching a solution, it also produces an important improvement in predicting the reactor performance.

Conclusions

The three phase reactor model presented here combined with previous kinetic studies satisfactorily describes most of the trends observed during the extensive experimental work performed by our group in the catalytic dehydrogenation of propane and the partial oxidation of n-butane. Results for both fluidized bed reactors (TZFBR and ICFBR) and both reactions are successfully described by the models presented.

Various parameters that could not be determined experimentally, such as the velocity of solid circulation or the oxidation state of the VPO catalyst, turned out to be among the most important reactor-related variables. Helped by the model, several improvements to the reactor may be made in future works. To sum up, the present work constitutes an important step forward in the understanding of fluidized bed reactors with two zones.

Notation

$C_{i,B}$, $C_{i,e}$ = concentration of the i compound in the bubble and the emulsion phases, respectively, [mol.m^{-3}]
f_w = fraction of wake in bubbles, -
F = feed flow (mol.s^{-1})
g = gravity acceleration, [m.s^{-2}]
h = bed height [cm]
h_0 = total bed height [cm]
h_b = height of the hydrocarbon feed point [cm]
$K_{B,e}$, $K_{e,B}$ = gas exchange coefficients between bubble and emulsion or vice-versa [s^{-1}]
K_{bc} = bubble-cloud exchange constant, [s^{-1}]
K_{ce} = cloud-emulsion exchange constant, [s^{-1}]
$K_{w,e}$, $K_{e,w}$ = solid exchange coefficient between wake and emulsion or vice-versa [s^{-1}]
P_h = percentage of hydrocarbon in the reactor total feed [%]
P_i = partial pressure of component i, bar
Q_i = volumetric flow rate of component i (cm^3 (STP)/s)
T = temperature [K],
r_i = reaction rate or mass transport rate in step i
$TZFBR$ = two zone fluidized bed reactor
$ICFBR$ = internal circulating fluidized bed reactor
u_0 = gas velocity [cm (STP)/min]
u_{mf} = minimum fluidization velocity [cm (STP)/min]
u_b = bubble velocity [m/s]
u_r = relative gas velocity (u/umf)
u_s = solid velocity [m/s]
W = amount of catalyst in the reactor [g]
W_r = amount of catalyst in the reacting zone [g]
d_b = bubble diameter [m]
db_0 = initial bubble diameter [m]
d_{Bm} = maximum bubble diameter [m]
D_t = reactor diameter [m]
D = diffusion coefficient (m^2/s)
α = fraction of bed in bubbles
$\theta_{subsurface}$ = concentration of oxygen in the catalyst lattice
$\theta_{surface}$ = concentration of lattice oxygen in the catalyst surface
λ_0 = concentration of adsorbed oxygen in the catalyst surface
ρ = solid density [kg/m^3]

Literature Cited

1. Gascón J, Téllez C, Herguido J, Menéndez M. A two zone fluidized bed reactor for catalytic propane dehydrogenation. *Chem Eng J.* 2005; 106:91–96.
2. Gascón J, Téllez C, Herguido J, Menéndez M. Fluidized bed reactors with two zones for maleic anhydride production: different configurations and effect of scale. *Ind Eng Chem Res.* 2005;44:8945–8951.
3. Sanfilippo D, Buonomo F, Fusco G, Lupieri M, Miracca, I. Fluidized bed reactors for paraffins dehydrogenation. *Chem Eng Sci.* 1992;47: 2313–2318.
4. Miracca I, Piovesan L. Light paraffins dehydrogenation in a fluidized bed reactor. *Catal Today.* 1999;52:259–269.
5. Arnold SC, Suciu GD, Verde L, Neri A. Use of fluid bed reactor for maleic anhydride from butane. *Hydrocarbon Proc.* 1985;September: 123–126.
6. Golbig KG, Werther J. Selective synthesis of maleic anhydride by spatial separation of n-butane oxidation and catalyst reoxidation. *Chem Eng Sci.* 1997;52:583–595.
7. Contractor RM. Dupont's CFB technology for maleic anhydride. *Chem Eng Sci.* 1999;54:5627–5632.
8. Arpentinier Ph, Cavani F, Trifirò F. The contribution of homogeneous reactions in catalytic oxidation processes: safety and selectivity aspects. *Catal Today.* 2005;99:15–22.
9. Contractor RM, Garnett DI, Horowitz HS, Bergna HE, Patience GS, Schwartz JT, Sisler GM. A new commercial scale process for n-butane

oxidation to maleic anhydride using a circulating fluidized bed reactor. *Stud Surf Sci Catal*. 1993;82:233–242.

10. Ramos R, Herguido J, Menéndez M, Santamaría J. Oxidation of hydrocarbons in an in situ redox fluidized bed reactor. *J Catal*. 1996; 163:218–221.

11. Soler J, López Nieto JM, Herguido J, Menéndez M, Santamaría J. Oxidative dehydrogenation of n-butane in a two-zone fluidized-bed reactor. *Ind Eng Chem Res*. 1999;38:90–97.

12. Rubio O, Grasa G, Herguido J, Abanades JC, Menéndez M. Oxidative dehydrogenation of butane in an interconnected fluidized bed reactor. *AIChE J*. 2004;50:1510–1522.

13. Callejas C, Soler J, Herguido J, Menéndez M, Santamaría J. Catalytic dehydrogenation of n-butane in a fluidized bed reactor with separate coking and regeneration zones. *Stud Surf Sci Catal*. 2000;130:2717–2722.

14. Herguido J, Menéndez M, Santamaría J. On the use of fluidized bed reactors where reduction and oxidation zones are presented simultaneously. *Catal Today*. 2005;100:181–189.

15. Soler J, Téllez C, Herguido J, Menéndez M, Santamaría J. Modelling of a two-zone fluidized bed reactor for the oxidative dehydrogenation of n-butane. *Powder Technol*. 2001;120:88–96.

16. Gascón J, Téllez C, Herguido J, Menéndez M. Propane dehydrogenation over a Cr$_2$O$_3$/Al$_2$O$_3$ catalyst: transient kinetic modelling of propane and coke formation. *Appl Catal: A General*. 2003;248:105–116.

17. Gascón J, Valenciano R, Téllez C, Herguido J, Menéndez M. A generalized kinetic model for the partial oxidation of n-butane to maleic anhydride under aerobic and anaerobic conditions. *Chem Eng Sci*. 2006;61:6385–6394.

18. Kunii D, Levenspiel O. *Fluidization Engineering*. 2nd ed. Boston: Butterworth-Heineman; 1991.

19. Behie LA, Kehoe P. The grid region in a fluidized bed reactor. *AIChE J*. 1973;19:1070-1072.

20. Davidson JF, Harrison D. *Fluidized Particles*. Cambridge: Cambridge University Press; 1963.

21. Rowe PN, Partridge PA. Proc. Particle movement caused by bubbles in fluidized beds: Symp. on the Interaction between Fluids and Particles. *Inst Chem Engr*. 1962;135–142.

22. Hoffmann AC, Janssen LPBM, Prins J. Particle segregation in fluidized binary-mixture. *Chem Eng Sci*. 1993;48:1583–1592.

23. Naimer NS, Chiba T, Nienow A. Parameter estimation for a solids mixing/segregation model for gas fluidized beds. *Chem Eng Sci*. 1982; 37:1047–1057.

24. Rubio O, Herguido J, Menéndez M. Oxidative dehydrogenation of n-butane on V/MgO catalysts. Kinetic study in anaerobic conditions. *Chem Eng Sci*. 2003;58:4619–4627.

25. Darton RC, Lanauze RD, Davidson JF, Harrison D. Bubble growth due to coalescence in fluidised beds. *Trans I ChemE*. 1997;55:274–280.

26. Horio M, Nonaka A. A generalized bubble diameter correlation for gas-solid fluidized beds. *AIChE J*. 1987;33:1865–1872.

27. Werther J, Wein J. Expansion behavior of gas fluidized beds in the turbulent regime. *AIChE Symp Ser*. 1994;90:31–44.

28. Hull AS, Chen Z, Fritz JW, Agarwal PK. Influence of horizontal tube banks on the behavior of bubbling fluidized beds. 1. Bubble hydrodynamics. *Powder Tech*. 1999;103:230–242.

29. Reid RC, Prausnitz JM, Poling BE. *The Properties of Gases and Liquids*. 4th ed. New York: McGraw-Hill; 1987.

30. Lim KS, Gururajan VS, Agarwal PK. Mixing of homogeneous solids in bubbling fluidized beds: theoretical modelling and experimental investigation using digital image analysis. *Chem Eng Sci*. 1993;48: 2251–2265.

31. Sane SU, Haynes HW, Agarwal PK. An experimental modelling investigation of gas mixing in bubbling fluidized beds. *Chem Eng Sci*. 1996;51:1133–1147.

32. Srinivasan SA, Sriramulu S, Kulasekaran S, Agarwal PK. Mathematical modelling of fluidized bed combustion. 2. Combustion of gases. *Fuel*. 1998;77:1033–1049.

33. Sriralmulu S, Sane S, Agarwal P, Mathews T. Mathematical modelling of fluidized bed combustion. 1. Combustion of carbon in bubbling beds. *Fuel*. 1996;75:1351–1362.

34. Shampine LF, Reichelt MW. The MATLAB ODE suite. *SIAM J Sci Comp*. 1997;18:1–22.

35. Shampine LF, Reichelt MW, Kierzenka JA. Solving Index-1 DAEs in MATLAB and Simulink. *SIAM Rev*. 1999;41:538–552.

36. Royo C, Menéndez M, Santamaría J. Kinetics of catalyst regeneration by coke combustion. I. Increased reaction rate due to the presence of chromium. *React Kinet Catal Lett*. 1991;44:445–450.

37. Stitt EH, Jackson SD, Shipley DG, King F. Modelling propane dehydrogenation in a rotating monolith reactor. *Catal Tod*. 2001;69:217–226.

38. Contractor RM, Bergna HE, Horowitz HS, Blackstone CM, Malone B, Torardi CC, Griffiths B, Chowdhry U, Sleight AW. Butane oxidation to maleic anhydride over vanadium phosphate catalysts. *Catal Today*. 1987;1:49–58.

39. Rodemerck U, Kubias B, Zanthoff, Wolf GU, Baerns M. The reaction mechanism of the selective oxidation of butane on (VO)$_2$P$_2$O$_7$ catalysts: the influence of the valence state of vanadium. *Appl Catal A: General*. 1997;153:217–231.

40. Mallada R, Menéndez M, Santamaría J. Use of membrane reactors for the oxidation of butane to maleic anhydride under high butane concentrations. *Catal Today*. 2000;56:191–197.

41. Alonso M, Lorences MJ, Pina MP, Patience GS. Butane partial oxidation in an externally fluidized bed-membrane reactor. *Catal Today*. 2001;67:151–157.